



Original Contributions

Y. Zhang, X. Xu.: Predicting doped Fe-based superconductor critical temperature using machine learning

Yun Zhang, Xiaojie Xu

North Carolina State University, Raleigh NC, USA

Predicting doped Fe-based superconductor critical temperature from structural and topological parameters using machine learning

Recently, Fe-based superconductors have shown promising properties of high critical temperature and high upper critical fields, which are prerequisites for applications in high-field magnets. Critical temperature, T_c , is an important characteristic correlated with crystallographic and electronic structures. By doping with foreign ions in the crystal structure, T_c can be modified, which however requires significant manpower and resources for materials synthesis and characterizations. In this study, we develop the Gaussian process regression model to predict T_c of doped Fe-based superconductors based on structural and topological parameters, including the lattice constants, volume, and bonding parameter topological index H_{31} . The model is stable and accurate, contributing to fast T_c estimations.

Keywords: Fe-based superconductor; Critical temperature; Crystal structure; Topological index; Gaussian process regression

1. Introduction

High magnetic fields are strongly sought in many application areas. Superconducting wires are among the top can-

didates as they allow for large electric current densities to flow without resistance. However, low temperature superconductors, such as NbTi and Nb₃Sn, can only generate magnetic fields up to 10.5 T and 20 T due to their upper critical fields being less than 25 T at 4.2 K. Thus, high-temperature superconductors with upper critical fields greater than 50 T, are promising candidates for magnet fabrication [1–6].

Iron-based superconductors have high critical temperature next to cuprates, an upper critical field above 50 T, a relatively high irreversibility field, and a high crystallographic symmetry, which are appropriate for fabrication of superconducting wires, tapes, and coated conductors. Among materials characteristics, critical temperature, T_c , is of most importance as it determines the applicability in practical situations. T_c is influenced by several factors, including lattice disorders and electronic structures. Generally, high- T_c superconductivity can be induced and tuned by varying dopant types and levels, where antiferromagnetism is diminished by carrier doping, structural modifications under external pressure, or chemical pressure via isovalent substitutions. For example, FeSe has the simplest structure among the known iron-based superconductors with a T_c of 8 K [7]. Combined with different doping mechanisms, a large variety of Fe-based superconductors

were synthesized, such as $AFeSe$ (A = alkali), $AeFe_2As_2$ (Ae = alkali-earth), and $LnOFeAs$ (Ln = lanthanide). Previous studies have indicated that changes in lattice constants reflect the expansion or contraction of the interlayer spacing of FeAs layers and local geometry of the $FePn(Ch)_4$ (Pn = pnictide, Ch = chalcogenides) tetrahedron [8]. Furthermore, inspired by the theoretical characterization of molecular branching that uses topological indices, the bonding parameter topological index H_{31} has been used to describe characteristics of the electronic structure of doped Fe-based superconductors. H_{31} is defined based on the relative atomic position, Pauling electronegativity, ionic radius, and valence state, which are strongly correlated with T_c [9].

Therefore, it is important to investigate the relationship between doping mechanisms and changes in critical temperature. However, this type of investigation is usually carried out by extensive experimental approaches, which involve resource-intensive and time-consuming synthesis and characterizations [10–16]. Recently, data-driven analysis has been proved to facilitate the understanding of the relationship between materials structures and performance by finding statistical correlations between physical attributes and property parameters [15–43]. This study sheds light on the relationship between superconducting transition temperature of iron-based superconductors and crystal cell structures via the Gaussian process regression (GPR) model. The model leads to accurate predictions of superconducting transition temperature and can be used to help understandings of superconducting transition temperature based on structural and topological parameters.

2. Methodology

The introduction of the methodology follows, e.g., [17–39]. GPRs are nonparametric kernel-based probabilistic models. Consider a training dataset, $\{(x_i, y_i); i = 1, 2, \dots, n\}$ where $x_i \in \mathbb{R}^d$ and $y_i \in \mathbb{R}$, from an unknown distribution. A trained GPR predicts values of the response variable y^{new} given an input matrix x^{new} . In the current study, x_i 's ($i = 1, 2, 3, 4$) are the lattice constants $-a$ and c , crystal cell volume $-V$, and bonding parameter topological index $-H_{31}$, y is the superconducting transition temperature, $T_c(K)$.

Recall a linear regression model, $y = x^T \beta + \varepsilon$, where $\varepsilon \sim N(0, \sigma^2)$. A GPR aims at explaining y by introducing latent variables, $l(x_i)$ where $i = 1, 2, \dots, n$, from a Gaussian process such that the joint distribution of $l(x_i)$'s is Gaussian, and explicit basis functions, b . The covariance function of $l(x_i)$'s captures the smoothness of y and basis functions project x into a feature space of dimension p .

A GP is defined by the mean and covariance. Let $m(x) = E(l(x))$ be the mean function and $k(x, x') = \text{Cov}[l(x), l(x')]$ the covariance function, and consider now the GPR model, $y = b(x)^T \beta + l(x)$, where $l(x) \sim GP(0, k(x, x'))$ and $b(x) \in \mathbb{R}^p$. $k(x, x')$ is often parameterized by the hyperparameter, θ , and thus might be written as $k(x, x' | \theta)$. In general, different algorithms estimate β , σ^2 , and θ for model training

and would allow specifications of b and k , as well as initial values for parameters.

The current study explores four kernel functions, namely Exponential, Squared Exponential, Matern 5/2, and Rational Quadratic, whose specifications are listed in Eqs. (1) – (4), respectively, where σ_l is the characteristic length scale defining how far apart x 's can be for y 's to become uncorrelated, σ_f is the signal standard deviation, $r = \sqrt{(x_i - x_j)^T \times (x_i - x_j)}$, and α is a positive-valued scale-mixture parameter. Note that σ_l and σ_f should be positive. This could be enforced through θ such that $\theta_1 = \log \sigma_l$ and $\theta_2 = \log \sigma_f$.

$$k(x_i, x_j | \theta) = \sigma_f^2 \exp\left(-\frac{r}{\sigma_l}\right) \quad (1)$$

$$k(x_i, x_j | \theta) = \sigma_f^2 \exp\left[-\frac{1}{2} \frac{(x_i - x_j)^T (x_i - x_j)}{\sigma_l^2}\right] \quad (2)$$

$$k(x_i, x_j | \theta) = \sigma_f^2 \left(1 + \frac{\sqrt{5}r}{\sigma_l} + \frac{5r^2}{3\sigma_l^2}\right) \exp\left(-\frac{\sqrt{5}r}{\sigma_l}\right) \quad (3)$$

$$k(x_i, x_j | \theta) = \sigma_f^2 \left(1 + \frac{r^2}{2\alpha\sigma_l^2}\right)^{-\alpha} \quad (4)$$

Similarly, four basis functions are investigated here, namely Empty, Constant, Linear, and Pure Quadratic, whose specifications are listed in Eqs. (5)–(8), respectively, where

$$B = (b(x_1), b(x_2), \dots, b(x_n))^T, \\ X = (x_1, x_2, \dots, x_n)^T, \text{ and } X^2 = \begin{pmatrix} x_{11}^2 & x_{12}^2 & \cdots & x_{1d}^2 \\ x_{21}^2 & x_{22}^2 & \cdots & x_{2d}^2 \\ \vdots & \vdots & \ddots & \vdots \\ x_{n1}^2 & x_{n2}^2 & \cdots & x_{nd}^2 \end{pmatrix} \\ B = \text{Empty Matrix} \quad (5)$$

$$B = I_{n \times 1} \quad (6)$$

$$B = [1, X] \quad (7)$$

$$B = [1, X, X^2] \quad (8)$$

To estimate β , σ^2 , and θ , the marginal log likelihood function in Eq. (9) is to be maximized, where $K(X, X | \theta)$ is the covariance function matrix given by

$$\begin{pmatrix} k(x_1, x_1) & k(x_1, x_2) & \cdots & k(x_1, x_n) \\ k(x_2, x_1) & k(x_2, x_2) & \cdots & k(x_2, x_n) \\ \vdots & \vdots & \ddots & \vdots \\ k(x_n, x_1) & k(x_n, x_2) & \cdots & k(x_n, x_n) \end{pmatrix}.$$

The algorithm first computes $\hat{\beta}(\theta, \sigma^2)$, maximizing the log likelihood function with respect to β given θ and σ^2 . It then obtains the β -profiled likelihood, $\log\{P(y|X, \hat{\beta}(\theta, \sigma^2), \theta, \sigma^2)\}$,

which is to be maximized over θ and σ^2 to compute their estimates.

$$\begin{aligned} \log P(y|X, \beta, \theta, \sigma^2) = & -\frac{1}{2}\{(y-B\beta)^T[K(X, X|\theta) \\ & + \sigma^2 I_n]^{-1}(y-B\beta)\} - \frac{n}{2}\log 2\pi \quad (9) \\ & -\frac{1}{2}\log|K(X, X|\theta) + \sigma^2 I_n| \end{aligned}$$

Table 1. Experimental data and different predictions.

Index	Sample	a (nm ⁻¹)	c (nm ⁻¹)	V (nm ³)	H_{31}	T_c (K)		
						Experimental	BPNN	GPR
1	LaFeO _{0.9} F _{0.1}	0.4032	0.8726	0.1419	1.3291	26.0	24.3	25.9980
2	LaFeAsO _{0.85}	0.4035	0.8715	0.1419	1.2431	31.2	28.5	31.1963
3	LaFe _{0.925} Co _{0.075} AsO	0.4038	0.8721	0.1422	1.3202	13.0	27.9	13.0036
4	LaFe _{0.96} Ni _{0.04} AsO	0.4035	0.8771	0.1428	1.3223	6.5	5.79	6.5036
5	La _{0.87} Sr _{0.13} FeAsO	0.4018	0.8713	0.1407	1.3170	25.0	24.1	24.9972
6	LaFe _{0.925} Ir _{0.075} AsO	0.4022	0.8707	0.1408	1.3339	11.8	16.8	11.8049
7	La _{0.8} Th _{0.2} FeAsO	0.4022	0.8662	0.1401	1.3855	30.3	28.4	30.2995
8	LaFeAs _{0.7} P _{0.3} O	0.4036	0.8708	0.1418	1.3828	10.0	10	10.0030
9	CeFeAsO _{0.84} F _{0.16}	0.3989	0.8631	0.1373	1.5516	41.0	35	40.9972
10	CeFeAsO _{0.85}	0.3979	0.8605	0.1362	1.4589	46.5	48.7	46.4976
11	CeFe _{0.9} Co _{0.1} AsO	0.3992	0.8603	0.1371	1.5453	11.3	26.4	11.3049
12	PrFeAsO _{0.89} F _{0.11}	0.3967	0.8561	0.1347	1.9081	52.0	50.7	51.9986
13	PrFeAsO _{0.85}	0.3968	0.8566	0.1349	1.7883	51.3	45.5	51.2987
14	Pr _{0.75} Sr _{0.25} FeAsO	0.3996	0.8660	0.1383	1.7202	16.3	16.1	16.3025
15	NdFeAsO _{0.82} F _{0.18}	0.3943	0.8521	0.1325	2.3641	51.0	48.9	50.9985
16	NdFeAsO _{0.85}	0.3953	0.8527	0.1332	2.2348	53.5	50.9	53.4982
17	Nd _{0.8} Sr _{0.2} FeAsO	0.3978	0.8642	0.1368	2.2921	13.5	11.7	13.5032
18	SmFeAsO _{0.8} F _{0.2}	0.3926	0.8479	0.1307	2.5988	54.0	54	53.9970
19	SmFeAsO _{0.85}	0.3897	0.8407	0.1277	2.4446	55.0	50.9	54.9974
20	SmFe _{0.9} Co _{0.1} AsO	0.3940	0.8470	0.1315	2.6447	17.2	27.2	17.2025
21	SmFe _{0.9} Rh _{0.1} AsO	0.3943	0.8450	0.1314	2.6387	10.0	13.5	10.0039
22	GdFeAsO _{0.85}	0.3903	0.8453	0.1288	2.2673	53.5	48.8	53.4976
23	Gd _{0.8} Th _{0.2} FeAsO	0.3916	0.8439	0.1294	2.3721	56.0	47.9	55.9978
24	TbFeAsO _{0.9} F _{0.1}	0.3902	0.8413	0.1281	2.9926	45.5	49.2	45.4995
25	Tb _{0.8} Th _{0.2} FeAsO	0.3881	0.8358	0.1259	2.7689	52.0	52.7	51.9985
26	Tb _{0.56} Ca _{0.44} FeAsO	0.3900	0.8423	0.1281	2.1568	15.6	32.3	15.6052
27	DyFeAsO _{0.9} F _{0.1}	0.3843	0.8284	0.1223	4.0594	45.3	44.8	45.2992
28	DyFeAsO _{0.8}	0.3859	0.8341	0.1242	3.3165	52.2	48.8	52.1984
29	HoFeAsO _{0.9} F _{0.1}	0.3830	0.8270	0.1213	5.0136	36.0	44.4	36.0005
30	HoFeAsO _{0.8}	0.3846	0.8295	0.1227	6.0413	50.3	46.3	50.2983
31	YFeAsO _{0.8}	0.3842	0.8303	0.1226	1.2318	46.5	46.2	46.4989
Minimum		0.3830	0.8270	0.1213	1.2318	6.5	5.8	6.5036
Mean		0.3949	0.8530	0.1331	2.2595	34.8	35.7	34.8161
Median		0.3953	0.8527	0.1332	2.1568	41.0	44.4	40.9972
Standard deviation		0.0066	0.0153	0.0068	1.1225	17.7	15.0	17.7006
Maximum		0.4038	0.8771	0.1428	6.0413	56.0	54.0	55.9978
CC w. T_c (K)		-58.75 %	-57.58 %	-58.88 %	36.42 %	-	94.05 %	99.99 %

Notes: Predictors include the lattice constants – a and c , crystal cell volume – V , and bonding parameter topological index – H_{31} . The target variable is the superconducting transition temperature, T_c (K). The BPNN (Back Propagation Neural Network) prediction is obtained from [44]. The GPR prediction is from the current study. All predictions are visualized in Fig. 3.

Model performance is assessed with the *CC* (correlation coefficient), *MAE* (mean absolute error), and *RMSE* (root mean square error).

3. Dataset

The experimental data in Table 1 (Columns 2–7) are from [9]. Predictors include the lattice constants – a and c , crystal cell volume – V , and bonding parameter topological index – H_{31} . The target variable is the superconducting transition temperature, $T_c(K)$. This dataset covers a wide range of doped Fe-based oxy-arsenides. Data are visualized in Fig. 1, which reveals nonlinear patterns modeled via the GPR.

4. Result

We investigate the relationship between model performance and the size of training data in Fig. 2, which shows the benefit of training the GPR with all observations. The stability of the GPR approach is confirmed by bootstrap validation analysis.

The final GPR model is reported in Fig. 3, whose performance is compared with that based on the BNPP (Back Propagation Neural Network) model [44]. The final GPR model is based on the Rational Quadratic kernel (Eq. (4)), Constant basis function (Eq. (6)), and standardized predictors, whose estimated parameters are: $\hat{\beta} = 37.0582$, $\hat{\sigma} = 0, 1994$, $\hat{\sigma}_l = 0.0935$, $\hat{\sigma}_f = 17.3098$, and $\hat{\sigma} = 0, 5223$. It is found that the GPR model provides more accurate superconducting

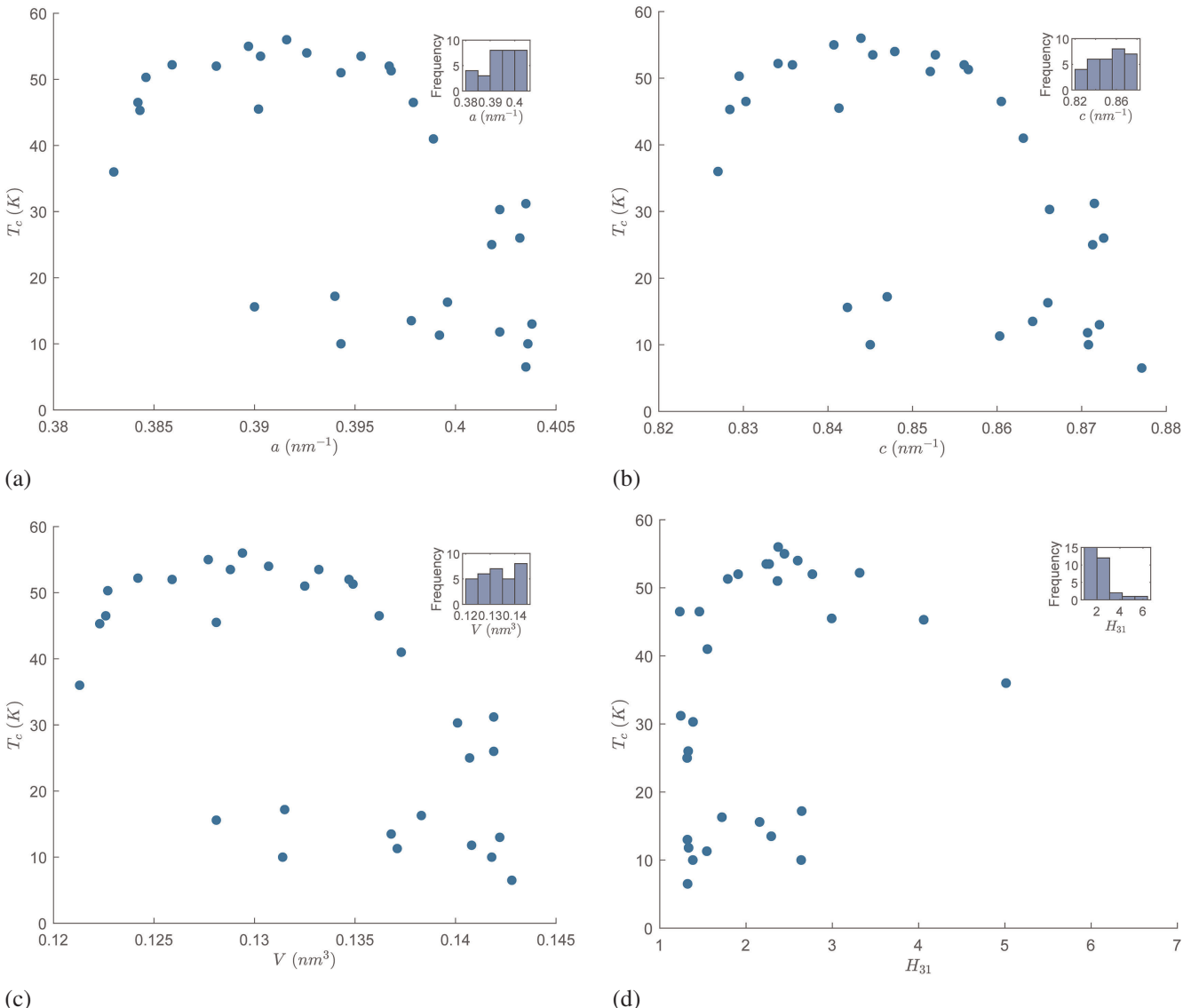


Fig. 1. Data visualization. Predictors include the lattice constants – a and c , crystal cell volume – V , and bonding parameter topological index – H_{31} . The target variable is the superconducting transition temperature, $T_c(K)$.

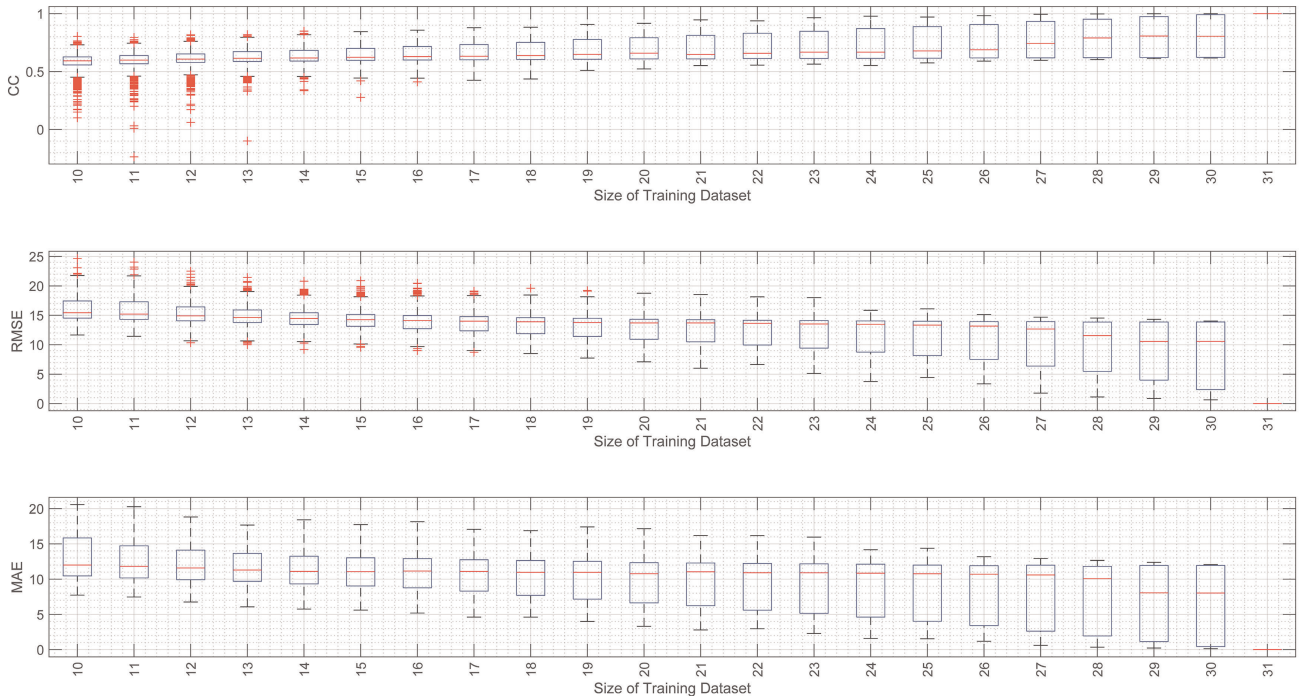


Fig. 2. Model performance and training data sizes. When the training dataset size is between 10 and 28, we draw 2000 random sub-samples from the whole sample without replacements to train models. When the training dataset size is 29, 30, or 31, we draw $31C_{29}$, $31C_{30}$, or $31C_{31}$ sub-samples from the whole sample without replacements based on exhaustive sampling to train models. Each trained model based on a certain sub-sample is utilized to score the whole sample and calculate the associated performance measurements. The GPR here uses the Rational Quadratic kernel and Constant basis function with standardized predictors. Provided a performance measure, box plots show the median, 25th percentile, and 75th percentile. The whiskers extend to the most extreme values (i.e. ± 2.7 standard deviation coverage) not considered as outliers, and the outliers are plotted using the “+” symbol.

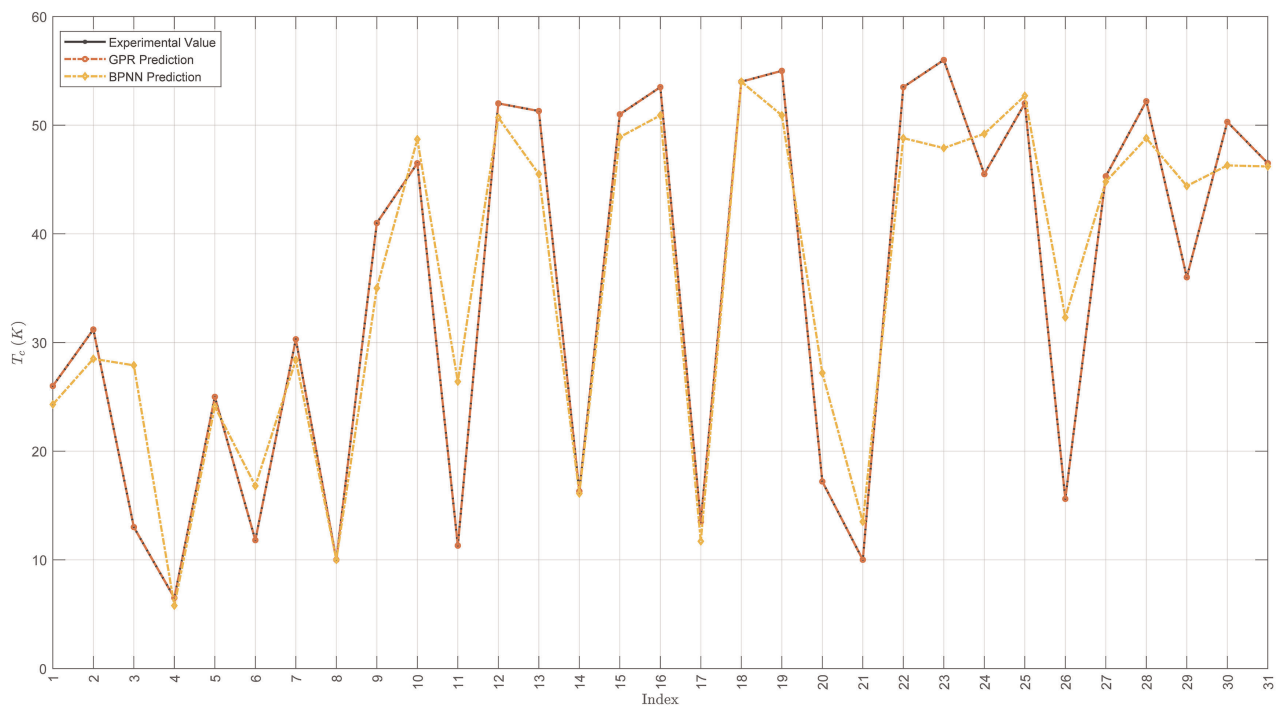


Fig. 3. Superconducting transition temperature predictions based on different models. The BNPP (Back Propagation Neural Network) prediction is obtained from [44]. The GPR model of the current study is constructed with the whole sample with the Rational Quadratic kernel, Constant basis function, and standardized predictors. It has a β of 37.0582, $\hat{\sigma}$ of 0.1994, $\hat{\sigma}_l$ of 0.0935, $\hat{\sigma}_f$ of 17.3098, and $\hat{\alpha}$ of 0.5223. Detailed numerical predictions based on different models are reported in Table 1 (Columns 8 and 9).

transition temperature predictions. Specifically, the *CC*, *RMSE*, and *MAE* based on the GPR model are 99.99 %, 0.0027, and 0.0024, respectively, while these measurements based on the BNPP model are 94.05 %, 6.1932, and 4.2906.

Given the small sample size (see Table 1) utilized, the prediction stability of the GPR is evaluated via bootstrap validation analysis in Fig. 4, which reveals that the modeling approach maintains high *CCs*, low *RMSEs*, and low *MAEs* across the bootstrap samples. This result suggests that the GPR might be generalized for superconducting transition temperature modeling based on larger samples for iron-based superconductors.

Table 2 shows that the Rational Quadratic kernel and Constant basis function are the optimal choice in terms of

performance measurements considered. This choice balances the simplicity and accuracy of the model.

5. Conclusion

We develop the Gaussian process regression (GPR) model to predict critical temperature, T_c , of doped Fe-based superconductors based on structural and topological parameters. The model is accurate and stable, which suggests the GPR's usefulness in modeling and understanding the relationship between crystal cell structures and superconducting transition temperature. The modeling exercise might also contribute to effective doping design of Fe-based superconductors for enhanced T_c .

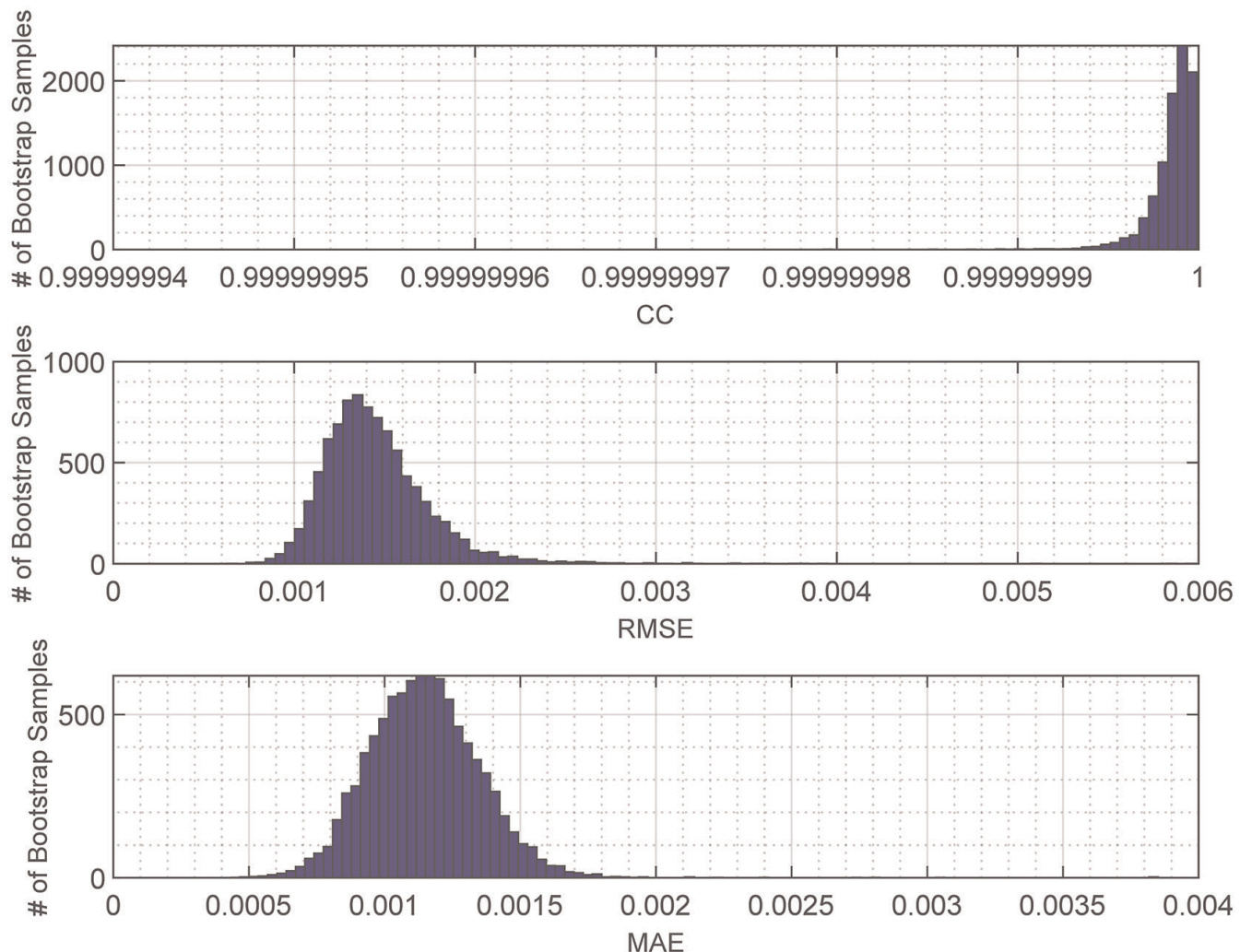


Fig. 4. Bootstrap analysis of GPR prediction stability. We draw 9000 bootstrap samples from the whole sample with replacements. Each bootstrap sample is utilized to train the GPR based on the Rational Quadratic kernel, Constant basis function, and standardized predictors, and calculate the associated performance measurements. The histograms plot distributions of the *CC*, *RMSE*, and *MAE* across the 9000 bootstrap samples, whose averages are 99.99 %, 0.0014, and 0.0011, respectively.

Table 2. GPR prediction sensitivities to kernel and basis function choices.

Kernel	Basis Function	CC	RMSE	<i>RMSE</i> <i>Sample Mean</i>	MAE	<i>MAE</i> <i>Sample Mean</i>
Rational Quadratic	Constant	99.99 %	0.0027	0.0079 %	0.0024	0.0070 %
	Exponential	86.34 %	10.1993	29.2947 %	8.9538	25.7174 %
Squared Exponential	Constant	62.37 %	13.8134	39.6753 %	11.8688	34.0898 %
	Matern52	65.07 %	13.5415	38.8945 %	11.7539	33.7600 %
Rational Quadratic	Empty	62.44 %	13.6667	39.2538 %	11.7718	33.8114 %
Rational Quadratic	Linear	66.17 %	13.0575	37.5041 %	10.8453	31.1503 %
Rational Quadratic	Pure Quadratic	74.69 %	11.5790	33.2575 %	8.8586	25.4440 %

Notes: The final GPR model is based on the Rational Quadratic kernel and Constant basis function, with predictors standardized.

References

- [1] J. Schwartz, C.C. Koch, Y. Zhang, X. Liu. Formation of bismuth strontium calcium copper oxide superconductors. US Patent: us9773962B2 (2017).
- [2] Y. Zhang, S. Johnson, G. Naderi, M. Chaubal, A. Hunt, J. Schwartz: Supercond. Sci. Technol. 29 (2016) 095012. DOI:10.1088/0953-2048/29/9/095012
- [3] Y. Zhang, C.C. Koch, J. Schwartz: Supercond. Sci. Technol. 29 (2016) 125005. DOI:10.1088/0953-2048/29/12/125005
- [4] Y. Zhang, C.C. Koch, J. Schwartz: Supercond. Sci. Technol. 27 (2014) 055016. DOI:10.1088/0953-2048/27/5/055016
- [5] J. Jiang, G. Bradford, S.I. Hossain, M.D. Brown, J. Cooper, E. Miller, Y. Huang, H. Miao, J.A. Parrell, M. White, A. Hunt, S. Sengupta, R. Revur, T. Shen, F. Kametani, U.P. Trociewitz, E.E. Hellstrom, D.C. Larbalestier: IEEE Trans. Appl. Supercond. 29 (2019) 1–5. DOI:10.1109/TASC.2019.2895197
- [6] T. Shen, E. Bosque, D. Davis, J. Jiang, M. White, K. Zhang, H. Higley, M. Turquetti, Y. Huang, H. Miao, U. Trociewitz: Sci. Rep. 9 (2019) 1–9. 46629–3. PMid:31308414; DOI:10.1038/s41598-019-
- [7] F.C. Hsu, J.Y. Luo, K.W. Yeh, T.K. Chen, T.W. Huang, P.M. Wu, Y.C. Lee, Y.L. Huang, Y.Y. Chu, D.C. Yan, M.K. Wu: Proc. Natl. Acad. Sci. U.S.A. 105 (2008) 14262–14264. DOI:10.1073/pnas.0807325105
- [8] X. Chen, P. Dai, D. Feng, T. Xiang, F.C. Zhang: Natl. Sci. Rev. 1 (2014) 371–395. DOI:10.1093/nsr/nwu007
- [9] Z. Min, S. Aimin, S. Lina, H. Peipei, L. Yanzhong, A. Xiaoqian, Z. Yongfu, Z. Dongye: Cryog. & Supercond. 4 (2012) 010.
- [10] Y. Wang, J. Zheng, Z. Zhu, M. Zhang, W. Yuan: J. Phys. D: Appl. Phys. 52 (2019) 345303. DOI:10.1088/1361-6463/ab1e2c
- [11] D. Qiu, W. Wu, Y. Pan, S. Xu, Z.M. Zhang, Z.L. Li, Z.Y. Li, Y. Wang, L. Wang, Y. Zhao, Z.W. Zhang: IEEE Trans. Appl. Supercond. 27 (2017) 1–5. DOI:10.1109/TASC.2017.2652538
- [12] P. Yang, K. Li, Y. Wang, L. Wang, Q. Wu, A. Huang, Z. Hong, G. Jiang, Z. Jin: IEEE Trans. Appl. Supercond. 29 (2019) 1–6. DOI:10.1109/TASC.2019.2900983
- [13] P. Yang, Y. Wang, D. Qiu, T. Chang, H. Ma, J. Zhu, Z. Jin, Z. Hong: IEEE Trans. Appl. Supercond. 28 (2018) 1–5. DOI:10.1109/TASC.2018.2810498
- [14] Y. Pan, J. Sheng, W. Wu, Y. Wang, W. Zeng, Y. Zhao, Z.W. Zhang, Z. Li, Z. Hong, Z. Jin: IEEE Trans. Appl. Supercond. 27 (2017) 1–5. DOI:10.1109/TASC.2017.2653358
- [15] W. Xu, Y. Wu, X. Gou: Comput. Methods Appl. Mech. Eng. 350 (2019) 535–553. DOI:10.1016/j.cma.2019.03.021
- [16] W. Xu, M. Jia, Z. Zhu, M. Liu, D. Lei, X. Gou: Mater. Des. 145 (2018) 108–115. DOI:10.1016/j.matdes.2018.02.065
- [17] Y. Zhang, X. Xu: Comput. Mater. Sci. 179 (2020) 109583. DOI:10.1016/j.commatsci.2020.109583
- [18] Y. Zhang, X. Xu: Physica C Supercond. Appl. 573 (2020) 1353633. DOI:10.1016/j.physc.2020.1353633
- [19] Y. Zhang, X. Xu: J. Magn. Magn. Mater. 512 (2020) 166998. DOI:10.1016/j.jmmm.2020.166998
- [20] Y. Zhang, X. Xu: Appl. Phys. A 126 (2020) 341. DOI:10.1007/s00339-020-03503-8
- [21] Y. Zhang, X. Xu: AIP Adv. 10 (2020) 035220. DOI:10.1063/1.5144241
- [22] Y. Zhang, X. Xu: Phys. Lett. A 384 (2020) 126500. DOI:10.1016/j.physleta.2020.126500
- [23] Y. Zhang, X. Xu: AIP Adv. 10 (2020) 045121. DOI:10.1063/5.0002448
- [24] Y. Zhang, X. Xu: Optik 217 (2020) 164808. DOI:10.1016/j.ijleo.2020.164808
- [25] Y. Zhang, X. Xu: RSC Adv. 10 (2020) 20646–20653. DOI:10.1039/D0RA03031G
- [26] Y. Zhang, X. Xu: ACS Omega 5 (2020) 15344–15352. DOI:10.1021/acsomega.0c01438
- [27] Y. Zhang, X. Xu: CrystEngComm 22 (2020) 6385–6397. DOI:10.1039/D0CE00928H
- [28] Y. Zhang, X. Xu: ChemistrySelect 5 (2020) 9999–10009. DOI:10.1002/slct.202002532
- [29] Y. Zhang, X. Xu: Met. Mater. Int. (2020). DOI:10.1007/s12540-020-00883-7
- [30] Y. Zhang, X. Xu: Phys. Chem. Miner. 47 (2020) 39. DOI:10.1007/s00269-020-01108-4
- [31] Y. Zhang, X. Xu: Shape Memory and Superelasticity (2020). DOI:10.1007/s40830-020-00303-0
- [32] Y. Zhang, X. Xu: Int. J. Quantum Chem. (2020). DOI:10.1002/qua.26480
- [33] Y. Zhang, X. Xu: J. Low Temp. Phys. (2020). DOI:10.1007/s10909-020-02545-9
- [34] Y. Zhang, X. Xu: J. Mater. Eng. Perform. 29 (2020) 6605–6616. DOI:10.1007/s11665-020-05146-5
- [35] Y. Zhang, X. Xu: Heliyon 6 (2020) e05055. DOI:10.1016/j.heliyon.2020.e05055
- [36] Y. Zhang, X. Xu: J. Supercond. Novel Magn. (2020). DOI:10.1007/s10948-020-05682-0
- [37] Y. Zhang, X. Xu: Mater. Technol. (2020). DOI:10.1080/10667857.2020.1830567
- [38] Y. Zhang, X. Xu: Chem. Phys. Lett. 760 (2020) 137993. DOI:10.1016/j.cplett.2020.137993
- [39] Y. Zhang, X. Xu: J. Mol. Graphics Modell. 103 (2021) 107796
- [40] Y. Zhang, X. Xu: Int. J. Thermophys. 41 (2020) 149. DOI:10.1007/s10765-020-02734-4
- [41] Y. Zhang, X. Xu: New J. Chem. (2020). DOI:10.1039/d0nj03868g
- [42] L. Xie, H. Zhong, Z. Du, J. Zhou: J. Quant. Spectrosc. Radiat. Transfer 241 (2020) 106744. DOI:10.1016/j.jqsrt.2019.106744
- [43] H. Zhong, L. Xie, J. Zhou, J. Quant. Spectrosc. Radiat. Transfer 247 (2020) 106952. DOI:10.1016/j.jqsrt.2020.106952
- [44] H. Zhang, Y. Zhang, Y. Zhu, Y. Xu, W. Shen, P. Wu, M. Cao, Z. Feng, Q. Li, J. Zhang: 2015 11th Int. Conf. Nat. Comput. (2015) 696–701. DOI:10.1109/ICNC.2015.7378075

(Received July 10, 2020; accepted September 9, 2020)

Correspondence address

Yun Zhang
North Carolina State University
Raleigh NC 27695
USA
E-mail: yzhang43@ncsu.edu

Xiaojie Xu
North Carolina State University
Raleigh NC 27695
USA
E-mail: xxu6@ncsu.edu

Bibliography

DOI 10.1515/ijmr-2020-7986
Int. J. Mater. Res. 112 (2021) 1; page 2–9
© 2021 Walter de Gruyter GmbH, Berlin/Boston, Germany
ISSN 1862-5282 · e-ISSN 2195-8556